

Towards Massive MIMO In-Band Full Duplex Radio

Patrick Rosson¹, Chandan Kumar Sheemar², Neharika Valecha² and Dirk Slock²

¹CEA, LETI, MINATEC Campus, F-38054 Grenoble, France

²Communication Systems Department, EURECOM, France
{patrick.rosson}@cea.fr , {sheemar,valecha,slock}@eurecom.fr

Abstract—In-band Full Duplex (IBFD) is a promising wireless transmission technology allowing to increase data rates by up to a factor of two, via simultaneous transmission and reception, but with a potential to increase system throughput even much more in cognitive radio and random access systems thanks to simultaneous transmission and sensing. The main ingredient allowing FD is Self Interference Cancellation (SIC). To reach the required high level of SIC, normally several SIC techniques need to be combined, such as antenna isolation or circulator attenuation, analog and digital SIC. Some of these techniques, esp. analog SIC, do not scale well with the number of antennas as required for Massive MIMO. In this paper we consider two promising directions, namely Hybrid SIC (HSIC), and MIMO SI Nulling (SIN), which is based on separate transmit and receive antenna arrays. HSIC can be realized with a number of SIC branches that scale linearly with the number of antennas. On the other hand, the MIMO SI channel can be designed to be of reduced rank, leading to reduced zero-forcing requirements for MIMO SIN. Both HSIC and MIMO SIN can be combined with digital SIC which does not introduce additional hardware. In this paper we present simulation and measurement results to capture some of the characteristics of both approaches.

Keywords— Full Duplex Self Interference cancellation/nulling, Hybrid SIC, Massive MIMO.

I. INTRODUCTION

The revolution in wireless communications has led to an increase in the data rate requirements and the number of users served in a limited wireless spectrum. This has caused a rising demand of communication systems that are spectrally efficient. In-band full-duplex (IBFD/FD) wireless radio, which has been proposed in [1], allows each node to transmit (Tx) and receive (Rx) simultaneously, has the potential to almost double the spectral efficiency and is one of the prominent candidates for 5G and beyond. It avoids the use of two independent channels for bi-directional communication, by allowing more flexibility in spectrum utilization, improving data security and reducing the air interface latency and delay issues.

However, IBFD systems suffer from severe self-interference (SI), which could be 110 dB higher than the receive signal power. SI cancellation (SIC) is not a trivial task, attributable to all the non-linearities and imperfections present in the transmitter chains [2]. But, the advancement in passive, active analog and active digital SIC techniques has made IBFD operation possible. Objective of these SIC techniques is to reduce SI near the noise floor to allow signal reception with high signal-to-self-interference-plus-noise-ratio. Analog cancellation is the fundamental block that suppresses SI by making sure that converters in the Rx chains can work

properly. Although, its complexity remains a major challenge as the number of antennas at the IBFD node increase. On the other hand, digital cancellation is a SIC technique with the lowest complexity but its performance strictly depends on how the analog cancelling stage performs.

As discussed in [3], the next generation base stations will deploy 64-256 antenna elements, which could make analog cancellation stage infeasible, owing to its high complexity and hardware cost. However, several architectures have already been proposed for IBFD operation, although their complexity at the analog SIC stage scales as $N_{rx}N_{tx}$, where N_{rx} and N_{tx} are the number of Rx and Tx antennas, respectively. In [4], a solution based on active regeneration of SI signal by an auxiliary transmitter which allows received SI power reduction and avoids LNA saturation is proposed. The transmitted auxiliary signal is derived from the transmitted baseband signal. A digital filter is also used to compensate for the differences between the leakage of main and auxiliary channels. After that, in the digital domain, a second digital filter is used to mitigate only the residual linear part of SI and the residual nonlinear part is not considered. Also the noises from two transmitters (i.e. main transmitter and auxiliary transmitter) are uncorrelated, which is a strong limitation for SIC. In [1], contrary to the solution proposed in [4], one antenna with circulator is used for both transmission and reception. The proposed solution is based on two filters: a digitally controlled RF filter and a digital filter. The analog filter is implemented with 16 delay lines, each with an attenuator that is digitally controlled. A 7 bit attenuator with 31.5 dB attenuation range is fitted to each of the 16 delay lines. Moreover, [1] also includes a nonlinear model of SI, which leads to better SI suppression. In [5], an extension of the architecture presented in [1] for the MIMO case is proposed. The same SIC solution of [1] is used to mitigate SI but additional analog filtering is also included to combat cross-talk.

Complexity of the aforementioned architectures is a serious challenge for upcoming massive MIMO IBFD scenarios. In contrast to these architectures, we propose a new hybrid SIC (HSIC) architecture which is able to regenerate all the SI and cross talk and its complexity scales linearly with the number of antennas. For correct analysis of the SI MIMO channel from the measured one, a new RF calibration algorithm to remove the effects of RF circuitry is presented. Finally, a new reduced complexity analog SI nulling (SIN) algorithm, which is motivated by the Vandermonde vector structure of uniform

linear array (ULA) response is proposed.

A. Contributions of this paper

- A new SIC architecture, which scales linearly with the number of antennas and will be prominent for upcoming massive MIMO IBFD scenarios.
- A new RF calibration algorithm, which allows to draw RF circuitry independent conclusions on the measured SI MIMO propagation channel.
- A new reduced complexity SIN algorithm for ULAs. Moreover, we also provide the upper bounds of SIN with different antenna array configurations.

Notation: In this paper, vectors and matrices are denoted with boldface lower-case and uppercase characters, respectively. The operators $E[\cdot]$, $\text{tr}\{\cdot\}$, $(\cdot)^H$, $(\cdot)^T$, $\|\cdot\|_F$ denote expectation, trace, Hermitian transpose, transpose and Frobenius norm, respectively. Tx and Rx may denote transmi/tter/ssion and receiv/e/er/ing.

II. IBFD ACTIVE RF MIMO HSIC

This section describes a new FD MIMO architecture using multiport SI regeneration. The model for the self-interferences in this new architecture is introduced and a solution is provided to in principle zero-force all self-interference at the receiver side. This section also provides a measured performance evaluation in a specific scenario.

A. MIMO D2RF HSIC Architecture

We propose a new architecture based on the Rice University solution [4], appropriate for MIMO FD transceivers. This architecture is able to regenerate all the self-interferences and mitigate them. In the MIMO context, self-interferences originate from the interactions between all Tx and all Rx chains. The proposed solution can be applied to the multi-antenna case in which antennas are shared between Tx and Rx chains via circulators. However, for the exposition here we shall focus on the case of separate Tx and Rx antenna arrays. For a $N_{tx} \times N_{rx}$ MIMO configuration, each receiver is affected by N_{tx} self-interferences coming from the N_{tx} transmitters. Therefore the FD transceiver must mitigate $N_{tx}N_{rx}$ self-interferences. A pure analog solution needs $N_{tx}N_{rx}$ SISO cancellers, which may need to be frequency-selective. E.g. for a 4×4 MIMO transceiver, the self-interferences come from 16 contributions that may result from filtering.

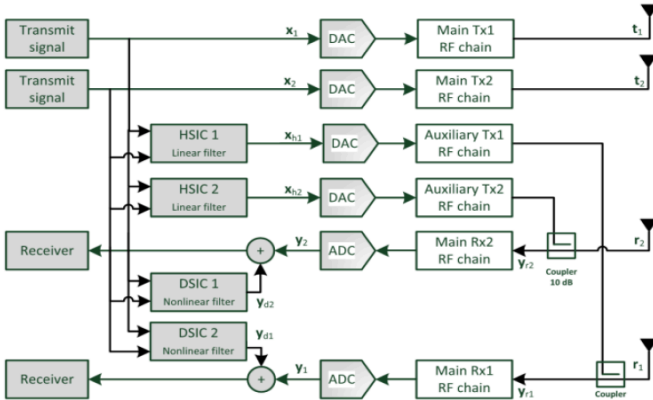


Fig. 1: 2×2 MIMO IBFD architecture with multiple HSIC and DSIC.

To reduce the complexity of an analog MIMO RF SIC, we decided to move analog filtering to the digital domain. This is done by using digital filters and auxiliary transmitters as in Fig. 1. The goal of the auxiliary Tx is to cancel the SI in the analog domain as much as possible, in any case enough for proper operation of the (ADCs in the) Rx chains. The output of each auxiliary Tx is a combination of signals coming from filtering the desired transmitter signals. In the end, digital MIMO SICs (DSICs) mitigate the remaining self-interference as discussed e.g. in [1]. Here we focus on the digital-to-RF (D2RF) hybrid SI cancellation (HSIC) for a MIMO configuration.

This MIMO D2RF HSIC solution is particularly well adapted for MIMO with a large number of antennas as it only requires N_{rx} HSIC branches, as compared to $N_{tx}N_{rx}$ branches in the case of analog SIC. To follow the Effective Isotropic Radiated Power (EIRP) regulation, the use of many Tx antennas implies power reduction per Tx antenna. This reduces the SI contribution level per Tx antenna.

This D2RF HSIC solution requires the use of additional Tx called auxiliary Tx in [6], which is a disadvantage. Depending on the degree of spatial multiplexing (number rank of useful streams) at the Tx, in a variation on this architecture, some available Tx antennas could be used not for data transmission but for active cancellation of SI towards the Rx antenna array, but we shall not discuss this variation here further.

B. Model

It is possible to define a $N_{rx} \times (N_{tx} + N_{rx})$ SI MIMO channel between all RF generators (i.e. main Tx chains and auxiliary Tx chains) and the Rx chains of the same transceiver. Ignoring non-linearities, and considering only SI signals, we can write the system equation in baseband in the frequency domain as:

$$\mathbf{y} = \begin{bmatrix} \mathbf{H}_{iac} & \mathbf{H}_{ih} \end{bmatrix} \begin{bmatrix} \mathbf{x} \\ \mathbf{x}_h \end{bmatrix} \quad (1)$$

where $\mathbf{y} = [y_1 \cdots y_{N_{rx}}]^T$ is the vector of Rx signal after HSIC cancellation and conversion (see Fig. 1), $\mathbf{x} = [x_1 \cdots x_{N_{tx}}]^T$ is the TX signal vector in the main Tx chain, $\mathbf{x}_h = [x_{h1} \cdots x_{hN_{rx}}]^T$ is the Tx signal vector for the auxiliary Tx chain, \mathbf{H}_{iac} represents the $N_{rx} \times N_{tx}$ MIMO SI channel for the main Tx chains (accounting for propagation from Tx to Rx antenna arrays and EM coupling between Tx and Rx RF arrays), whereas \mathbf{H}_{ih} represents the $N_{rx} \times N_{rx}$ MIMO SI channel for the auxiliary Tx chains in the HSIC branches (accounting for the explicit coupling from auxiliary Tx to Rx RF arrays and their EM coupling also).

We can also define a $N_{rx} \times N_{tx}$ MIMO digital filter \mathbf{H}_{hsic} . This digital filter massages the actual Tx signal \mathbf{x} into an appropriate input \mathbf{x}_h for the auxiliary Tx chains in the HSIC branches before subtraction in the RX chains and SI cancellation. We have the relation

$$\mathbf{x}_h = \mathbf{H}_{hsic} \mathbf{x}. \quad (2)$$

C. MIMO SI Channel Estimation

This section proposes a simple approach to estimate the self-interference MIMO channel (i.e. the $N_{rx}(N_{tx} + N_{rx})$ sub-

channels). The problem is similar to classical MIMO channel estimation. The main difference is that time and frequency synchronisation is not necessary in this configuration as the same oscillator and the same sampling frequency are used for all the transmitters and all the receivers.

A reference signal is transmitted on each transmitted port sequentially. During this phase, the two synchronised receivers estimate all the sub-channels. The self-interference MIMO channel is estimated like in TDMA (orthogonal transmission scheme). We follow here the dimensions $N_{rx} = N_{tx} = 2$ of Fig. 1. The four transmitted and received complex signals (IQ) versus time are shown in Fig. 2 and Fig. 3 respectively, exhibiting the time multiplexed pilots. This estimation phase is the most straightforward and was implemented in the simulator discussed further, but a non-orthogonal approach can also be used to reduce its duration. Of course, adaptive filtering approaches can also be used to determine \mathbf{H}_{hsic} directly without SI channel estimation (as for the digital SIC).

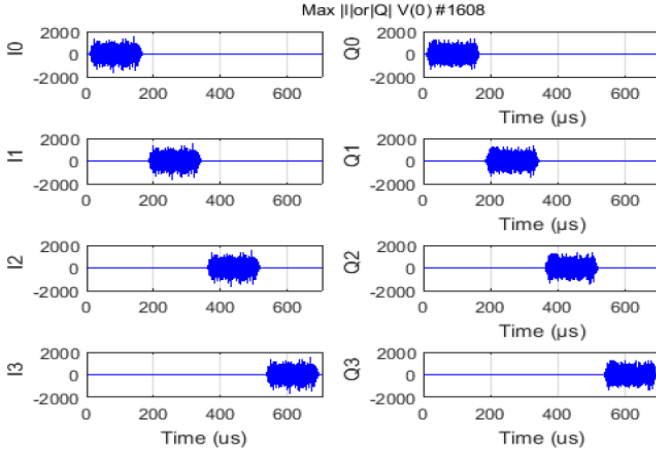


Fig. 2: Estimation phase - Transmitted pilot signal on each Tx.

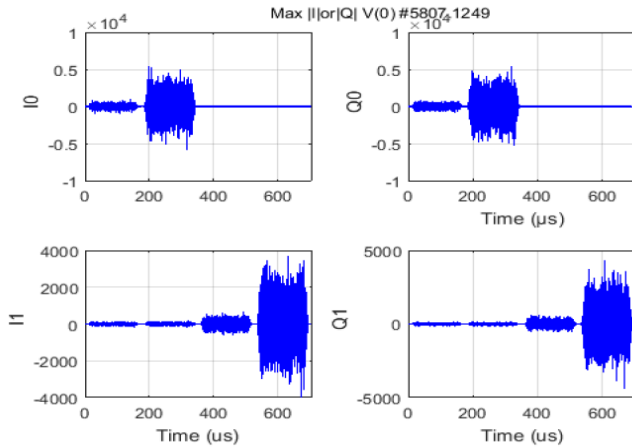


Fig. 3: Estimation phase Received signal on each Rx.

D. Zero Forcing HSIC Solution

In the SISO configuration, when the transceiver has only one Tx and one Rx antenna, there is only one self-interference and the HSIC can easily be computed [6], [7]. In the MIMO configuration the problem is a bit more complex. We should find the HSIC filters which minimize the SI power of the two

received signals. The filtering can be narrowband (i.e. only one complex coefficient per sub-channel) or wideband (i.e. FIR with several coefficients per sub-channel). This depends on delay spread of the MIMO SI channel and the RF bandwidth. Substituting (2) into (1) gives $\mathbf{y} = (\mathbf{H}_{iac} + \mathbf{H}_{ih} \mathbf{H}_{hsic}) \mathbf{x}$. Hence, in order to zero-force all the SI effect of \mathbf{x} on \mathbf{y} , the HSIC filter obviously needs to be chosen as

$$\mathbf{H}_{hsic} = -\mathbf{H}_{ih}^{-1} \mathbf{H}_{iac}. \quad (3)$$

In wideband filtering, to reach good SI mitigation, the delay spread of \mathbf{H}_{hsic} needs to be sufficiently large.

E. HSIC Simulations results

We simulated wideband filtering (up to 4 FIR coefficients per subchannel). The ZF solution is computed based on the 8 MIMO SI subchannel estimations (FIR of length 4). Figure 4 shows the transmitted signals and the self-interference when the HSIC is not applied (in which case we have antenna isolation only) and when it is applied. The antenna isolation is around 30 dB. HSIC MIMO allows around 30 dB of additional cancellation, up to the noise floor in this scenario. The left and right subfigures correspond to Rx chains 1 and 2, respectively.

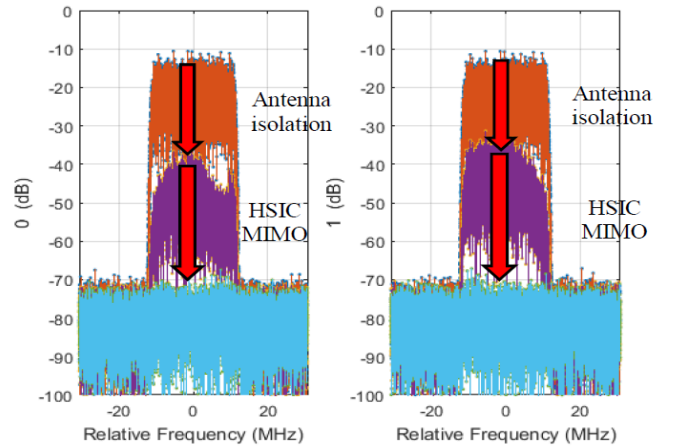


Fig. 4: MIMO HSIC Performance.

III. IBFD MIMO SI NULLING

In this section, we first model the internal MIMO SI channel between ULAs with the near field LOS model and propose a new iterative RF calibration algorithm for correct analysis of SI MIMO channel from the measured channel. We perform measurements with different antenna array configurations and our objective would be to achieve a low rank SI MIMO channel, which leads to reduced ZF constraints. Finally, a reduced complexity analog SIN algorithm, which exploits the banded nulling structure and motivated by the Vandermonde vector structure of ULA response is proposed.

A. RF Calibration and LoS Near Field MIMO Channel Model

We consider an OFDM IBFD system with a total of N_s sub-carriers. The measured SI MIMO channel at each subcarrier n can be written as:

$$\mathbf{H}[n] = \mathbf{R}[n] \mathbf{C}[n] \mathbf{T}[n] + \mathbf{V}[n] \quad (4)$$

where $\mathbf{C}[n]$ and $\mathbf{V}[n]$ are the internal SI MIMO propagation channel and measurement noise, respectively. $\mathbf{R}[n]$ and $\mathbf{T}[n]$

denote the calibration matrices, which represent the transfer function of RF circuitry in Tx and Rx chains. As discussed in [8], these matrices are diagonal, which is also true for our case. We consider the near field line-of-sight (LoS) model for $\mathbf{C}[n]$, with each of its elements given by:

$$c_{i,j}[n] = \frac{\alpha[n]}{d_{i,j}^\gamma} e^{-j\beta d_{i,j}}, \quad (5)$$

where $\beta = 2\pi f_n$ is the phase constant with subcarrier frequency f_n , d denotes distance, $\alpha[n]$ is a constant, γ is the pathloss factor and subscript (i, j) denotes the j -th Tx and the i -th Rx antennas, respectively. The measured channel $\mathbf{H}[n]$ not only depends on the internal SI MIMO propagation channel, but also on the RF circuitry in the Tx and Rx chains. Therefore, to remove the effect of RF circuitry from the measured channel, we present a new iterative algorithm for RF calibration which leads us closer to the actual internal SI MIMO propagation channel. This allows us to draw conclusions which depend only on the antenna configuration and the effects of RF circuitry are removed. As the RF circuitry does not alter the phase of transmitted signals but just their amplitudes, we only need the absolute calibration factors. To obtain these factors in $\mathbf{R}[n]$ and $\mathbf{T}[n]$, we use the least square (LS) fitting criterion at the level of $\mathbf{C}[n]$ instead of $\mathbf{H}[n]$, which reflects the decorrelated Gaussian modeling error on $\mathbf{C}[n]$. By estimating these absolute calibration factors directly from $\mathbf{H}[n]$, we apply them on $\mathbf{C}[n]$. For calibration purposes, we minimize the average LS fit over subcarriers $n - q_s : n + q_s$, i.e. $2q_s + 1$ subcarriers, with $q_s \in [1, n]$. The objective function we consider is:

$$\min_{\alpha[n], \mathbf{T}[n], \mathbf{R}[n]} \sum_{m=\max(1, n-q_s)}^{\min(N_s, n+q_s)} \|\mathbf{R}[n]\mathbf{H}[m]\mathbf{T}'[n] - \mathbf{C}'[m]\|_F^2, \quad (6)$$

where $\mathbf{C}[m] = \alpha[m]\mathbf{C}'[m]$ and $\mathbf{T}'[n] = \alpha[n]\mathbf{T}[n]$ is the reparameterization of $\mathbf{T}[n]$ in terms of $\alpha[n]$. Optimization of (6) is done at each subcarrier with alternating minimization approach according to the LS fitting w.r.t $\mathbf{T}'[n]$ and $\mathbf{R}[n]$. For the sake of simplicity, optimal solution for $\mathbf{R}[n]$ is also obtained in two steps. Firstly, we solve for its unconstrained solution $\mathbf{R}'[n]$, which is later scaled to recover $\mathbf{R}[n]$. By assuming $\gamma = 1$, the LS cost solution for (6) w.r.t $\mathbf{T}'[n]$ and $\mathbf{R}[n]$ (in two steps) at iteration k can be obtained as follows:

$$\mathbf{T}'_k[n] = \text{diag}\left(\sum_m \mathbf{H}^H[m]\mathbf{R}'_k[n]\mathbf{C}'[m]\right) \left(\text{diag}\left(\sum_m \mathbf{H}^H[m]\mathbf{R}'_k[n]\mathbf{R}'_k[n]\mathbf{H}[m]\right)\right)^{-1}, \quad (7)$$

$$\mathbf{R}'_k[n] = \text{diag}\left(\sum_m \mathbf{C}'[m]\mathbf{T}'_k[n]\mathbf{H}^H[m]\right) \left(\text{diag}\left(\sum_m \mathbf{H}[m]\mathbf{T}'_k[n]\mathbf{T}'_k[n]\mathbf{H}^H[m]\right)\right)^{-1}, \quad (8)$$

$$\mathbf{R}_k[n] = \mathbf{R}'_k[n] \sqrt{N_{rx}} / \|\mathbf{r}'_k[n]\|_2, \quad (9)$$

where $\mathbf{r}'_k[n] = \text{diag}(\mathbf{R}'_k[n])$, N_{rx} denotes the number of Rx antennas and the scaling factor $\sqrt{N_{rx}} / \|\mathbf{r}'_k[n]\|_2$ forces the values of $\mathbf{R}[n]$ to fluctuate around 1, leading to the true physical RF calibration factors. By alternating between (7)-(9)

at each subcarrier until convergence, we get the optimal $\mathbf{R}[n]^*$ and $\mathbf{T}'[n]^*$. To recover $\alpha[n]^*$, $\mathbf{T}[n]^*$ the following equations can be used:

$$\alpha[n]^* = \sqrt{N_{tx}} / \|\mathbf{t}'[n]^*\|_2, \quad (10)$$

$$\mathbf{T}[n]^* = \alpha[n]^* \mathbf{T}'[n]^*, \quad (11)$$

where $\mathbf{t}'[n]^* = \text{diag}(\mathbf{T}'[n]^*)$ and N_{tx} denotes the number of Tx antennas. We then compute the calibrated internal SI MIMO channel $\hat{\mathbf{C}}[n]$ as:

$$\hat{\mathbf{C}}[n] = \alpha[n]^* \mathbf{C}'[n]. \quad (12)$$

The complete iterative procedure for RF calibration at each subcarrier is presented in Algorithm 1.

Algorithm 1 RF Calibration Algorithm

At each subcarrier n , initialize $\mathbf{R}[n], \mathbf{T}'[n] = \mathbf{I}$.
Initialize $\mathbf{C}'[n]$ according to (5) with $\alpha[n], \gamma[n] = 1$.
Repeat until convergence:

- 1) Update $\mathbf{T}'_k[n]$ according to (7).
- 2) Update $\mathbf{R}'_k[n]$ using (8).
- 3) Update $\mathbf{R}_k[n]$ from (9).

After convergence, from $\mathbf{T}'[n]^*$ get $\alpha[n]^*$, $\mathbf{T}[n]^*$ and then $\hat{\mathbf{C}}[n]$ according to (10)-(12), respectively.

B. Reduced Complexity Analog SI Nulling

We now consider a generic IBFD communication system with ULAs equipped with N_{tx} Tx and N_{rx} Rx antennas. The SI MIMO channel is denoted with $\mathbf{C} \in \mathbb{C}^{N_{rx} \times N_{tx}}$ and we assume $N_{tx} < N_{rx}$. For our LoS model, we first assume that the near field effects of amplitude variation with distance and phase variation are negligible. Let $\mathbf{x} = [1, a, a^2, \dots]$ be a Vandermonde vector, which represents the array response of a ULA array. Then, to null \mathbf{x} we can use a Toeplitz matrix $\mathcal{T}([1, -1/a, 0, \dots])$ with $[1, -1/a, 0, \dots]$ as its first row, such that $\mathcal{T}([1, -1/a, 0, \dots])\mathbf{x} = 0$. Under the far field assumption, the channel matrix \mathbf{C} between ULAs, for array response of one array towards the centre of the other array, can be written as a rank 1 product of two Vandermonde vectors. At the Rx side, \mathbf{C} looks like a Vandermonde vector and hence $\mathcal{T}([1, -1/a, \dots, 0])$ in front of \mathbf{C} captures its singular part. Motivated by this idea, for SIN we propose that at the receiver side a SIN filter $\mathbf{N} \in \mathbb{C}^{N_{rx} - 2 \times N_{rx}}$ with the Toeplitz structure $\mathcal{T}([1, -1/a, 0, \dots])$ should be applied. If the Rx array is a uniform rectangular array (URA), under the far field approximation, \mathbf{C} is still rank 1, as it is a product of Rx and Tx antenna array responses. But the URA response at the Rx side should be written as a Kronecker product $\mathbf{v}_V \otimes \mathbf{v}_H$ of two ULA responses of vertical and horizontal dimensions, respectively. Moreover, if we vectorize the URA response $\mathbf{V} = \mathbf{v}_V \mathbf{v}_H^T$ as $\mathbf{v} = \text{vec}(\mathbf{V}) = \mathbf{v}_H \otimes \mathbf{v}_V$, then to null \mathbf{v} we have to use two Toeplitz SIN filters \mathbf{N}_V and \mathbf{N}_H . We can also increase the number of non-zero upper diagonals in one or the other SIN filter, or both, to change the dimensions. Even with URA, we can decide to use only one SIN filter e.g. \mathbf{N}_v , which may also work. The Kronecker Toeplitz SIN structure with two filters

given by $(\mathbf{N}_V \otimes \mathbf{N}_H)\mathbf{v} = 0$ leads to nulling the product of two zeros. However, this over nulling could be justified by the fact that the Vandermonde structure we assume is approximate due to near field effects. Therefore, for the actual \mathbf{C} , the Kronecker Toeplitz SIN filter structure with two filters would perform better in nulling the SI for URAs.

Aforementioned reasoning is the motivation for a banded nulling structure that we impose on the SIN filter \mathbf{N} . Nevertheless, in reality we don't impose the Toeplitz structure on it, but we let its elements on the non-zero upper diagonals to be arbitrary complex numbers, which are then optimized for nulling purpose. For our problem formulation, we choose only one SIN filter with two super diagonals to be non zero. The objective function for SIN that we optimize is the following:

$$\min_{a_i, b_i} \|\mathbf{N}\mathbf{C}\|_F^2, \text{ for } a_i, b_i \in \mathbb{C} \text{ and } i = 1, \dots, N_{rx} - 2. \quad (13)$$

where a_i and b_i are the elements of the first and the second super diagonals in row i . To solve (13), we rewrite the matrix \mathbf{C} as a $(N_{rx} - 2)N_{tx} \times 2(N_{rx} - 2) + 1$ sparse matrix \mathbf{C}_s (15) and reformulate (13) as a quadratic cost function of complex variables with a linear constraint:

$$\begin{aligned} \min_{\mathbf{x}} \quad & \|\mathbf{C}_s \mathbf{x}\|^2 \\ \text{s.t.} \quad & \mathbf{e}_1^T \mathbf{x} = 1 \end{aligned} \quad (14)$$

where \mathbf{e}_1 is the first standard basis vector of the Euclidean space and $\mathbf{x} = [1, a_1, \dots, a_{N_{rx}-2}, b_1, \dots, b_{N_{rx}-2}]^T$ contains the complex coefficients of \mathbf{N} .

$$\mathbf{C}_s = \begin{bmatrix} c_{1,1} & c_{2,1} & \mathbf{0} & c_{3,1} & \mathbf{0} \\ \vdots & \vdots & \vdots & \vdots & \vdots \\ c_{N-2,1} & \mathbf{0} & c_{N-1,1} & \mathbf{0} & c_{N,1} \\ \vdots & \vdots & \vdots & \vdots & \vdots \\ c_{1,M} & c_{2,M} & \vdots & c_{3,M} & \vdots \\ \vdots & \mathbf{0} & \vdots & \mathbf{0} & \vdots \\ c_{N-2,M} & \mathbf{0} & c_{N-1,M} & \mathbf{0} & c_{N,M} \end{bmatrix} \quad (15)$$

The solution for (14) can be obtained as:

$$\mathbf{x} = \frac{1}{\mathbf{e}_1^T (\mathbf{C}_s^T \mathbf{C}_s)^{-1} \mathbf{e}_1} (\mathbf{C}_s^T \mathbf{C}_s)^{-1} \mathbf{e}_1. \quad (16)$$

The vector \mathbf{x} provides the optimal complex coefficients to be stacked in the two upper diagonals of \mathbf{N} , which null the SI. However, as the dimension of Rx signal after SIN cannot be higher than N_{tx} , (13) with its reformulation (14), should be iterated K times to reduce the size of \mathbf{N} to $L \times N_{rx}$, with $L = N_{rx} - K$ and $L \leq N_{tx}$. At each iteration k for $k = 1, \dots, K$, the row i of \mathbf{N} which produces the highest norm for $\mathbf{A} = \mathbf{N}\mathbf{C}$ should be removed by restructuring $\mathbf{C}_s(k)$ with less columns, which correspond to the removal of coefficients a_i and b_i of \mathbf{N} . By doing so, we suppress the $N_{tx} - L$ dominant dimensions of the SI MIMO channel. The complete reduced complexity analog SIN algorithm for SIN is given in Algorithm 2.

IV. SIMULATION & MEASUREMENT RESULTS

In this section, simulation results are presented for the proposed RF calibration algorithm applied to a 4×4 IBFD OFDM system with $N_s = 296$ subcarriers. Then to evaluate the performance of our reduced complexity analog SIN algorithm, we present simulation results for a generic IBFD system with

Algorithm 2 Reduced complexity analog SIN algorithm

Initialize $\mathbf{C}_s(0)$ according to (15).

for $k = 1, \dots, K$

- 1) $\mathbf{C}_s(k) = \mathbf{C}_s(k-1)$.
- 2) Evaluate $\|\mathbf{N}\mathbf{C}_s(k)\|_F^2$.
- 3) Update $\mathbf{C}_s(k)$ by removing its columns to remove the row in \mathbf{N} which produces the highest norm for \mathbf{A} .
- 4) Solve for new $\mathbf{x}(k)$ with updated $\mathbf{C}_s(k)$ in (16).
- 5) Stack $\mathbf{x}(k)$ in the upper diagonals of \mathbf{N}

end

ULAs equipped with 4 Tx and 6 Rx antennas and with one SIN filter \mathbf{N} of size 4×6 and 3×6 .

A. RF Calibration Results

We considered a 4×4 IBFD OFDM MIMO communication system. The experiments were performed on a setup consisting of a USRP N310 software defined radio and Huawei patch antenna cards as part of the OAI platform, Eurecom. Each card has four patch antennas shaped like an H. We observed during our experiments that the channel is also affected by the orientation of the antenna cards and thus we perform the channel measurements for two orientations H and \perp of the Tx and the Rx. All the measurements are taken indoors at the carrier frequency $f_c = 2.585$ GHz.

For SI MIMO channel measurement, we transmit an OFDM frame of bandwidth 5 MHz with 296 subcarriers. The channel measurements are taken for three different configurations of the Tx and Rx antennas as shown in Figure 5. The distances d_{ij} are a function of the distance between the Tx and the Rx P , the horizontal inter-antenna spacing δ_1 and the vertical inter-antenna spacing δ_2 . The measurements are done for different values of P .

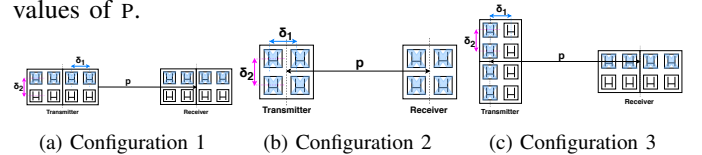
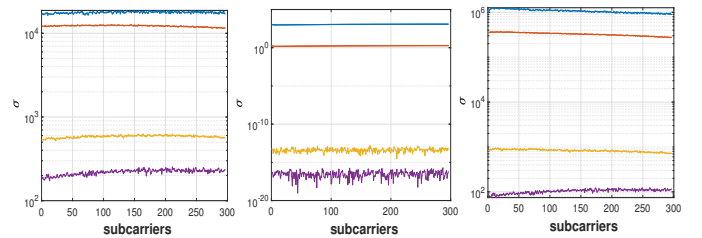


Fig. 5: Transmitter and Receiver Antenna Layout

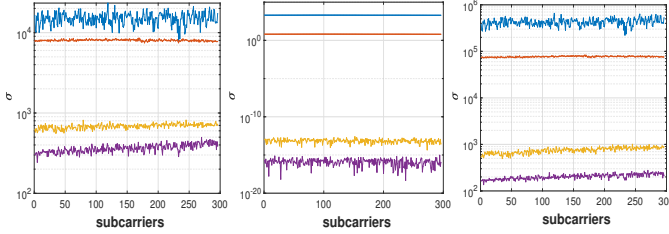


(a) Measured Channel \mathbf{H} (b) Internal Channel \mathbf{C} (c) Calibrated Channel $\hat{\mathbf{C}}$

Fig. 6: SVP of the SI MIMO channel for configuration 3 with $P = 47$ cm and with Tx and Rx in orientation H and \perp , respectively.

Figures 6-7 show the singular value profile (SVP) for 296 subcarriers of the measured SI MIMO channel \mathbf{H} , the SI MIMO propagation channel \mathbf{C} generated according to the near field LoS model (5) and the calibrated SI MIMO channel $\hat{\mathbf{C}}$ obtained by using Algorithm 1. Figure 6 corresponds to the Tx

and Rx in configuration 3 with $P=47$ cm and Tx in orientation H and Rx in orientation \perp . Figure 7 shows the SVP of the channels for Tx and Rx in configuration 3 with $P=37.1$ cm and Tx and Rx in orientation H. It can be observed from the Figures that the measured channel can be approximated as rank 2, which is evident after the calibration process in $\hat{\mathbf{C}}$.



(a) Measured Channel \mathbf{H} (b) Internal Channel \mathbf{C} (c) Calibrated Channel $\hat{\mathbf{C}}$
 Fig. 7: SVP of the SI MIMO channel for configuration 3 with $P = 37.1$ cm and with Tx and Rx in orientation H.

We do not include the results for configuration 1 and 2 as the measured (and calibrated) channels for the considered antenna layouts resulted to be full rank.

B. Reduced Complexity SIN Results

Now, we present the simulation results for our SIN approach applied to an IBFD system with ULAs consisting of 4 Tx antennas and 6 Rx antennas. The internal SI MIMO propagation channel \mathbf{C} is generated according to the near filed LoS model (5) with $\gamma, \alpha = 1$. For evaluation of the proposed SIN algorithm, we assume the additive signal model $\mathbf{y} = \mathbf{C}\mathbf{s} + \mathbf{v}$, where \mathbf{s} is the Tx signal and \mathbf{v} is the intended Rx signal. We further assume that the signals \mathbf{s} and \mathbf{v} are white. However, in reality they are not white but this assumption allows us analyze the upper bounds for the proposed SIN Algorithm 2 for ULAs with different configurations shown in Fig. 5. For evaluation purposes, we define the metric self-interference-to-signal-ratio ($SISR$) as the ratio of effective SI power to effective Rx signal power. The $SISR$ before and after the SIN filter \mathbf{N} is denoted with $SISR_i$ and $SISR_o$, respectively. For the assumed signal model above, $SISR_i$ and $SISR_o$ can be calculated as:

$$SISR_i = \frac{\sigma_s^2 \text{tr}(\mathbf{C}\mathbf{C}^H)}{\sigma_v^2 (N_{rx} + 2)} \quad SISR_o = \frac{\sigma_s^2 \text{tr}(\mathbf{N}\mathbf{C}\mathbf{C}^H\mathbf{N}^H)}{\sigma_v^2 \text{tr}(\mathbf{N}\mathbf{N}^H)} \quad (17)$$

where σ_s^2 and σ_v^2 denote the variances of \mathbf{s} and \mathbf{v} , respectively.

Figure 8 shows the ratio $SISR_o/SISR_i$ as a function of distance, for $\mathbf{C} 6 \times 4$ and $\mathbf{N} 4 \times 6$ and 3×6 . It is evident that the proposed SIN algorithm works better with configuration 1. There is no significant variation in $SISR_o/SISR_i$ for configuration 3 as the distance between Tx and Rx antennas increases but for configuration 1 the ratio decays rapidly which demonstrates the nulling of SI. It is also evident in Figure 8 the advantage of reducing the Rx signal dimension by 1 with $K = 3$, which removes the most dominant dimension of the SI signal for both configurations. Results are not reported for configuration 2 because we considered only one SIN filter and configuration 2 requires two SIN filters \mathbf{N}_V and \mathbf{N}_H to null SI in vertical and horizontal dimensions to achieve good results.

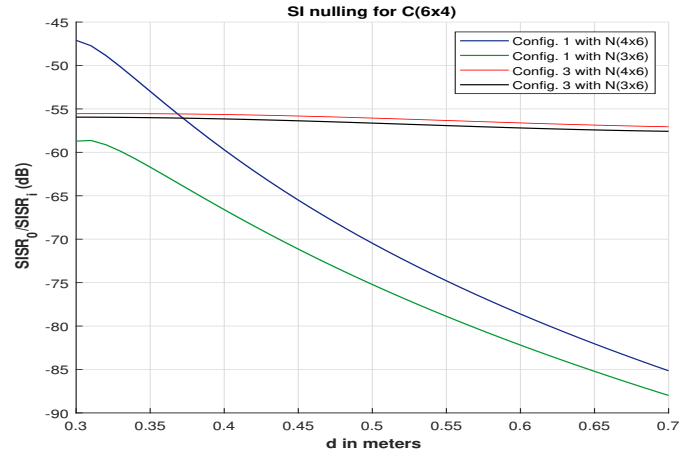


Fig. 8: Results obtained with the SI nulling algorithm for configuration 1 and 3 for $\mathbf{C}(6 \times 4)$, $\mathbf{N}(4 \times 6)$ and $\mathbf{N}(3 \times 6)$.

V. CONCLUSIONS

In this paper we presented a new HSIC architecture which is prominent for the upcoming IBFD massive MIMO communication scenarios, as its complexity at the analog cancelling stage scales linearly with the number of Rx antennas. A new RF calibration algorithm is proposed, which is later used for the analysis of SI MIMO channel from the measured channel with USRP N310. Results demonstrate that we achieved SI MIMO channel of rank 2 with configuration 3 for a 4×4 FD system. Finally, a reduced complexity analog SI nulling algorithm is proposed and the upper bounds for a 4×4 FD system with ULAs are presented.

ACKNOWLEDGEMENTS

The research leading to these results received funding from the French National Research Agency (ANR) via the DUPLEX project. EURECOMs research is also partially supported by its industrial members: ORANGE, BMW, Symantec, SAP, Monaco Telecom, iABG, by the projects MASS-START (French FUI) and EU ITN project SPOTLIGHT.

REFERENCES

- [1] D. Bharadia, E. McMillin, and S. Katti, "Full Duplex Radios," in *Proc. ACM SIGCOMM*, 2013.
- [2] S. Li and R. D. Murch, "Full-Duplex Wireless Communication using Transmitter Output based Echo Cancellation," in *Proc. IEEE Global Telecom's Conf. (GLOBECOM)*, 2011.
- [3] 3GPP Technical Report V14.1.0, "Study on Scenarios and Requirements for Next Generation Access Technologies," 2017.
- [4] M. Duarte, C. Dick, and A. Sabharwal, "Experiment-Driven Characterization of Full-Duplex Wireless Systems," *IEEE Trans. Wireless Comm's*, Nov. 2012.
- [5] D. Bharadia and S. Katti, "Full Duplex MIMO Radios," in *Proc. 11th USENIX Symp. Networked Systems Design and Implementation (NSDI)*, 2014.
- [6] A. Debar, P. Rosson, D. Dassonville, and V. Berg, "Flexible In-Band Full-Duplex Transceivers Based on a Modified MIMO RF Architecture," in *Proc. Int'l Conf. Cognitive Radio Oriented Wireless Networks (CROWN)*. Springer, 2016.
- [7] P. Rosson, D. Dassonville, X. Popon, and S. Mayrargue, "SDR Based Test Bench to Evaluate Analog Cancellation Techniques for In-Band Full-Duplex Transceiver," in *Proc. 5th Int'l Workshop Cloud Technologies and Energy Efficiency in Mobile Communication Networks (CLEEN)*. IEEE, 2017.
- [8] K. Gopala and D. Slock, "Antenna Array Absolute Self-Calibration and Application to Separate Tx/Rx Array Full Duplex MIMO," in *Proc. IEEE Globecom Workshops*. IEEE, 2017.